# INFRARED THERMOGRAPHY TECHNIQUES FOR BOUNDARY LAYER STATE VISUALISATION

William Davis, Nicholas R. Atkins
Whittle Laboratory
University of Cambridge, UK

## ABSTRACT

The rapid decarbonisation needed for power generation and aviation to have sustainable futures requires step changes in aerothermal technology. This necessitates working in large design spaces where the state of the boundary layer and its resulting loss and heat transfer characteristics are difficult to predict. Standard measurement techniques such as thin-film gauges and oil flow visualisation are intrusive and time consuming, so there is a need for improved testing methods to diagnose changes and develop physical understanding.

Infrared (IR) thermography has found wide use in aerothermal research due to its ability to measure surface temperatures in a range of conditions. IR measurements of the boundary layer state have been demonstrated in many experiments, however there is little information available on the best practices for fast and accurate measurements. IR transition measurements rely on temperature differences between laminar and turbulent regimes, which are dependent on the thermal characteristics of the system. This paper shows how a 1D heat transfer analysis can be used to maximise the signal-to-noise ratio (SNR) of IR measurements. This can improve measurement quality and minimise complexity, effort and intrusion on the flow. Experimental work is used to validate the analysis and demonstrate the value of IR in rapid testing.

## INTRODUCTION

Mayle [1] discussed the importance of laminar-turbulent transition in turbomachinery for accurate understanding of loss and heat transfer. Given the difficulty in predicting transition in design it is often necessary to measure it when there is uncertainty in the boundary layer state, either on as designed parts or to enhance predictive capability with correlations.

This paper demonstrates the use of infrared thermography as a method for rapid diagnosis of boundary layer state. Low-speed flows require active heating while high-speed flows can utilise differences in recovery temperature between boundary layer states. Experimental and analytical analyses are carried out to determine best practice in both regimes. Examples of the capabilities of IR are shown and the limitations of the method discussed.

### Boundary layer state measurement

There are a wide variety of measurement methods capable of detecting changes in boundary layer state, from a wool tuft to pitot and hot wire probes. This paper focuses on full field measurement methods to characterise the boundary layer over an entire surface, something that is necessary to move quickly in large design spaces. Two extreme examples are discussed here.

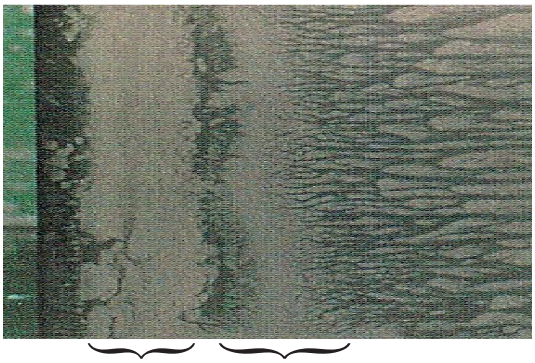


(a) Oil flow visualisation [2].

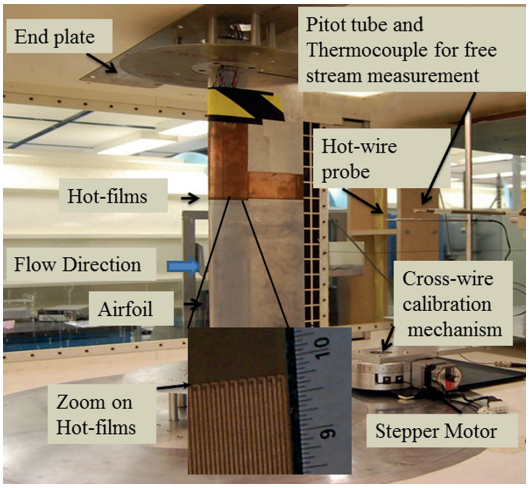


(a) Hot films [3].

**Figure 1:** Transition measurement methods.

Oil flow visualisation is a common and low-cost surface visualisation method. An example is shown in Fig. 1(a), where oil has been used to detect a laminar separation bubble and subsequent

turbulent reattachment, seen by the pooling of oil in the separation bubble and critical lines either side. Oil flow visualisation can be done quickly, but only once a suitable oil mixture has been formulated. It requires careful interpretation of images and must be cleaned and reapplied between operating points, making repeated testing such as a Reynolds number sweep slow. Measurement resolution is limited by oil properties and the non-zero thickness of the oil makes it intrusive, which can result in early transition compared to a clean flow.

The other extreme in complexity is thin film gauges for unsteady skin friction measurements. An application of thin-films is shown in Fig. 1(b). Transition and separation can be detected from relative changes in skin friction and thin films can be used to measure unsteady effects due to their short response times. In the Fig. 1(b) thin films give chord-wise changes in properties but average in the span-wise direction, removing 3D effects. The time and costs of instrumenting an aerofoil with thin-films and their low spatial resolution makes them ill-suited for use in rapid testing.

### Infrared thermography

Infrared thermography has been used for boundary layer visualisation since the 1970s, such as by Peake et al. [4]. Modern cameras with high spatial resolution and frame rates make detailed flow visualisation, including in the rotating frame as demonstrated by Mori et al. [5].

An example IR visualisation of transitional flow is shown in Fig. 2. IR measures surface temperatures, which can be used to infer boundary layer state from a difference in heat transfer coefficient. In Fig. 2, as in the rest of this paper, hotter regions are lighter and cooler regions are darker. The turbulent streak and transition across the full span further downstream are seen by a temperature differential from the increased heat transfer of the turbulent flow. As the visualisation relies on differences, calibration of the IR camera is not necessary. IR can provide full field visualisation of boundary layer state faster and easier than oil flow visualisation. It gives high resolution, non-intrusive, repeatable measurements and can be done without stopping between operating points.

In low Mach number flows it is necessary to heat or cool the surface to generate a temperature difference from changes in heat transfer. The test in Fig. 2 used a heater embedded in the test model, which is why laminar regions are hotter. The need for heating is a limit on infrared methods, but it is not always necessary to install a heater in the model, with techniques such as heat lamps or transient heating or cooling possible. Measurement quality is governed by the thermal properties of the system. If the test model is a thermally conductive material an insulating layer is needed between it and the flow. Without this the temperature difference between laminar and turbulent regions is conducted away. The best practice for such a set-up is not clear in the literature, with authors such as Joseph et al. [6] including the insulator without explanation. Determining the best practice and assessing the limits of IR is the focus of the rest of this paper.

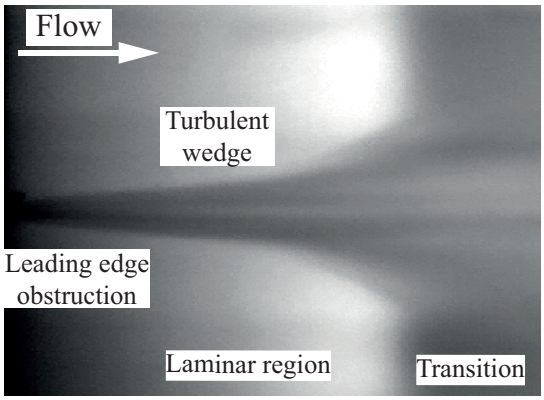


**Figure 2:** IR visualisation of a turbulent streak.

### Paper outline

The paper is split into three parts. The first part uses a 1D heat transfer analysis to demonstrate how measurements can be optimised. The second part focuses on a low Mach number test case to validate the 1D model, including a case study on rapid testing with IR. The final section previews current work at high Mach numbers with industrial applications.

## THEORETICAL ANALYSIS

To demonstrate the possible problems and optimisations in IR measurements a simplified theoretical analysis is used. The overall layout of the 1D model is shown in Fig. 3. The fluid is assumed to have a uniform free stream temperature. A heat transfer coefficient $h$ encapsulates the thermal resistance of the boundary layer. The surface is insulating with thickness $d$, below which is a thermally conductive substrate. The thermal properties of the insulating layer are the main parameter for investigation in this work.

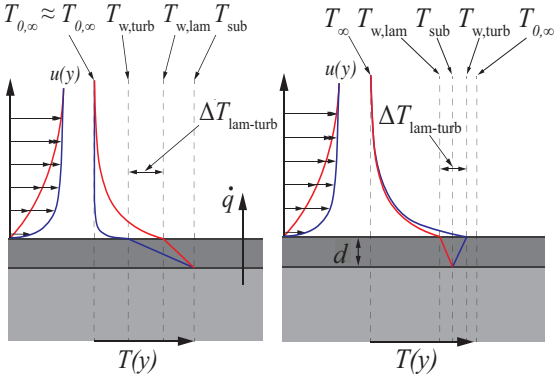


(a) Low-speed (b) High-speed

**Figure 3:** One-dimensional heat transfer model.

Two flow regimes are considered, labelled as low-speed and high-speed. There is some recovery temperature between the free stream and the boundary layer given by

$$T_{rec} = \left(1 + r\frac{\gamma - 1}{2}M_{\infty}^2\right)T_{\infty} \qquad (1)$$

where $r$ is the recovery factor. On a zero-pressure-gradient flat plate in air $r$ is around 0.85 for a laminar boundary layer and 0.90 for a turbulent one [7], so there is a temperature difference $\Delta T_{\text{lam-turb}}$ over transition from the recovery temperature. A temperature difference can also be generated with a heat flux through the wall. Different heat transfer coefficients between laminar and turbulent boundary layers also results in a $\Delta T_{\text{lam-turb}}$. These two concepts are shown in Figs. 3(a) and 3(b).

In this work a high-speed flow is taken to be one where the recovery temperature difference alone without active heating is enough to detect transition with IR. Low-speed flow is any other case where active heating is needed to draw out a $\Delta T_{\text{lam-turb}}$. The boundary between the two depends on the minimum required signal-to-noise ratio, the ratio of $\Delta T_{\text{lam-turb}}$ and the noise-equivalent temperature difference (NETD) of the IR camera. Equation 1 shows that the high-speed regime requires high Mach numbers and depends on the stagnation temperature of the flow.

The effect of insulator and flow properties on $\Delta T_{\text{lam-turb}}$ is determined by considering 1D heat transfer between the substrate and flow. Heat flux through the insulator and boundary layer is given by

$$\dot{q} = \frac{\lambda}{d}(T_{\text{sub}} - T_{\text{w}}) = h(T_{\text{w}} - T_{\text{rec}}) \qquad (2)$$

where λ is the thermal conductivity of the insulator. A Biot number is defined as the ratio of the thermal resistances of the insulator and boundary layer.

$$Bi = \frac{hd}{\lambda} \qquad (3)$$

Rearranging Eq. 2 gives the wall temperature as

$$T_{\text{w}} = T_{\text{sub}} - \frac{Bi}{Bi+1}(T_{\text{sub}} - T_{\text{rec}}) \qquad (4)$$

$h$ increases over transition, as does the Biot number, giving $Bi_{\text{lam}}$ and $Bi_{\text{turb}}$. $T_{\text{sub}}$ is assumed to be constant. $\Delta T_{\text{lam-turb}}$ is given by

$$\Delta T_{\text{lam-turb}} = \left|T_{\text{w,lam}} - T_{\text{w,turb}}\right| \qquad (5)$$

The following analysis considers the effect of changing $d/\lambda$ on $\Delta T_{\text{lam-turb}}$.

**Low-speed flow**

Low-speed flows have wide ranging use cases such as future electric aircraft and sports aerodynamics. With a negligible recovery temperature difference Eq. 5 simplifies to give a normalised laminar-turbulent temperature difference of

$$\frac{\Delta T_{\text{lam-turb}}}{T_{\text{sub}} - T_{0,\infty}} = \frac{Bi_{\text{turb}}}{Bi_{\text{turb}}+1} - \frac{Bi_{\text{lam}}}{Bi_{\text{lam}}+1} \qquad (6)$$

This can be differentiated to find the conditions that maximise the SNR. To understand the effect of the flow, flat plate correlations are used, given by

$$Nu = \begin{cases} 0.332Re^{1/2}Pr^{1/3} & \text{laminar} \\ 0.0296Re^{4/5}Pr^{1/3} & \text{turbulent} \end{cases} \qquad (7)$$

These give a good representation of the heat transfer behaviour over a transitional region. When applied to Eq. 6 the optimal Biot number with respect to the laminar heat transfer coefficient is

$$Bi_{\text{lam,opt}} = \sqrt{\frac{h_{\text{lam}}}{h_{\text{turb}}}} \propto Re^{-0.15} \qquad (8)$$

where $h_{\text{lam}}/h_{\text{turb}}$ is the ratio of heat transfer coefficients at transition and depends on conditions at that point. This shows that the optimal value of insulator $d/\lambda$ depends on the type of flow.

Figure 4 shows curves of Eq. 6. The locus of Eq. 8 is also shown. The optimum exists but is relatively flat in the direction of higher Biot numbers. This allows thick, low conductivity insulators such as 3D printed polymer to be used. The troublesome region is with low Biot numbers, where the SNR drops sharply.

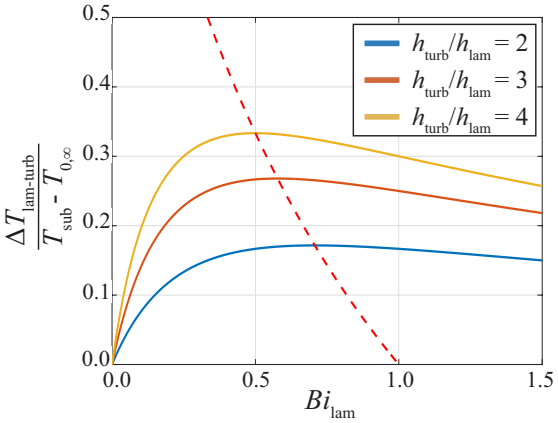


**Figure 4:** Analytic variation in $\Delta T_{\text{lam-turb}}$ with varying insulator Biot number for low-speed flows. The red dashed line indicates the locus of the maximum points of the curves, given by Eq. 8.

Consider as an example a flow with $h_{\text{turb}}/h_{\text{lam}}=3$ and $h_{\text{lam}} = 10\,\text{Wm}^{-2}\text{K}^{-1}$, representative of a Reynolds number around $1.5\times10^5$. A typical insulator for a rapid test is an adhesive polymer film or a rapid prototype shell, with thermal conductivity of $0.2\,\text{Wm}^{-1}\text{K}^{-1}$. Heating is limited by the material, so is at most 20K above the free stream. A 0.1mm film achieves a $\Delta T_{\text{lam-turb}}$ of 0.2K, not detectable by a moderately priced IR camera, while a 2mm shell gives a $\Delta T_{\text{lam-turb}}$ of 2.5K, which is usable for visualisation. This demonstrates the need to consider the thermal properties of the insulator to avoid poor measurements.

**High-speed flow**

In a high-speed flow with a stagnation temperature close to ambient, which is common in stationary turbomachinery and aircraft aerodynamic testing, the recovery temperature tends to cool the surface. The higher recovery temperature of a turbulent boundary layer means it appears hotter in IR compared to laminar regions.

When not fixed by active heating $T_{\text{sub}}$ can vary throughout a test. Analysis here assumes that the substrate has a high thermal mass and remains at the ambient condition of the free stream stagnation temperature. Applying this condition to Eqs. 4 and 5

results in the curves shown in Fig. 5. Similar features are seen compared to Fig. 4, with a sharp rise in SNR at low Biot numbers to a peak value. The major difference is at Biot numbers around one the SNR goes to zero. There is an interplay between heat transfer and recovery temperature effects. In turbulent regions the higher heat transfer acts to decrease wall temperature, while the higher recovery temperature acts to increase it. At low Biot numbers heat transfer is dominant, so laminar regions are hotter. As Biot number increases there is a crossover where $\Delta T_{\text{lam-turb}}$ is zero. At high Biot numbers the system approaches an adiabatic state, so $\Delta T_{\text{lam-turb}}$ tends to the recovery temperature difference. It is critical to avoid Biot numbers around one where the SNR is close to zero.

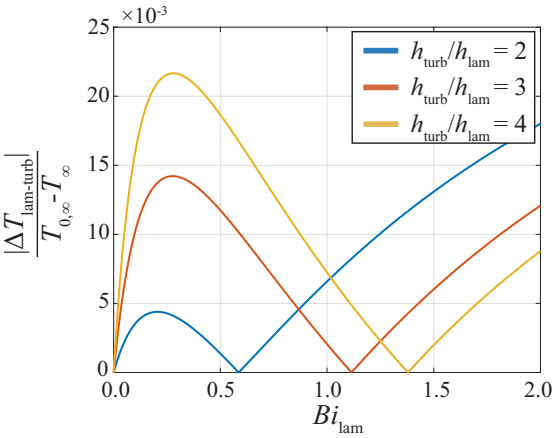


**Figure 5:** Analytic variation in $\Delta T_{\text{lam-turb}}$ with varying insulator Biot number for high-speed flows.

In reality the substrate temperature tends to drop during a test, resulting in a transient problem. At short time scales the wall is close to adiabatic, taking the recovery temperature. As heat transfer takes place between the flow and the substrate the effect seen in Fig. 5 kicks in. At long time scales the substrate will cool until it reaches a thermal equilibrium with the flow. A fully immersed blade is close to adiabatic, but if one side is exposed to ambient conditions then heat transfer continues at a rate governed by the thermal resistance of the test apparatus.

## LOW-SPEED EXPERIMENTS

The previous section demonstrates pitfalls in the use of IR in low and high-speed testing. This section discusses experimental work done to validate the low-speed analysis and demonstrate the use of IR for rapid testing.

### Experimental set up

To validate the 1D analysis an experimental set up is designed to generate a range of flow features and reflect realistic use of IR in testing. The overall experimental design is shown in Fig. 6. The working section is 458mm×688mm and is connected to a low-speed wind tunnel at the Whittle Laboratory. A 300mm chord, 430mm span 2D NACA 0018 aerofoil is chosen as it displays both bypass and separation bubble transition mechanisms at available Reynolds numbers up to $4.5\times10^5$ [8]. The aerofoil incidence is set with a rotating mount on the tunnel wall. The aerofoil is too large relative to the tunnel for accurate values of free stream behaviour, but still shows the desired aerodynamic features. Minimal 3D flow is seen at the end walls and does not affect IR measurements.

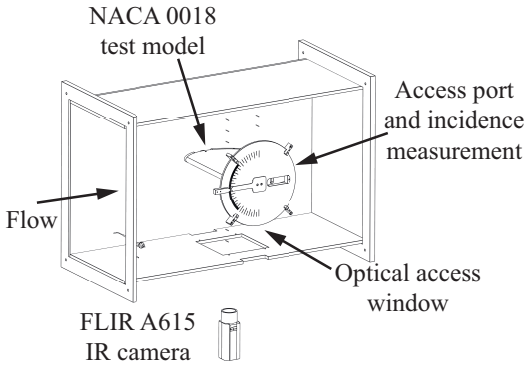


**Figure 6:** CAD view of the low-speed test section used for validation.

A FLIR A615 IR camera is used for visualisation. The A615 is a relatively inexpensive camera with a resolution of 640×480 pixels, a spectral range of 7.5-14μm and an NETD of 50mK. A 25° field of view lens is used for a full view of the aerofoil from beneath the working section. Optical access is provided by a window in the floor. A basic calibration from a heated virtual black body is used as the qualitative nature of IR visualisation negates the need for rigorous temperature calibration.

Details of the NACA 0018 test model are shown in Fig. 7. The model is constructed from two aluminium parts. One of these parts has the NACA 0018 profile machined into its surface, while the other has a series of 8 steps along its span. An SLA printed shell interlocks with the steps, acting as the insulator discussed in the previous section. The steps increase in thickness along the span from 2mm to 6mm. All 8 thicknesses are tested at once, allowing for rapid data collection. Insulation is also added to the aluminium side in the form of 0.1mm black film, allowing Biot numbers to be increased from zero. The aerofoil surface is painted matte black to increase emissivity, which helps in IR by increasing the apparent temperature of the body and reducing reflections.

The aerofoil is heated internally with 240V silicone heater mats delivering up to 400W, with internal insulating foam to force heat through the surface. The heaters are controlled with a pulse-width modulation PID loop to hold the aluminium at a fixed temperature and avoid overheating the insulating shell, which starts to deform above 54°C [9]. There are 7 thermocouples embedded in the aluminium for control and to ensure heating is uniform. Data was collected with $T_{\text{sub}}$ at 15K above ambient unless stated otherwise.

The shell has 51 0.3mm diameter surface pressure tappings along the chord to compare

pressure profiles with IR. Pressure tappings in the tunnel wall, an inlet pitot-static system and an inlet thermocouple are used for flow measurement.

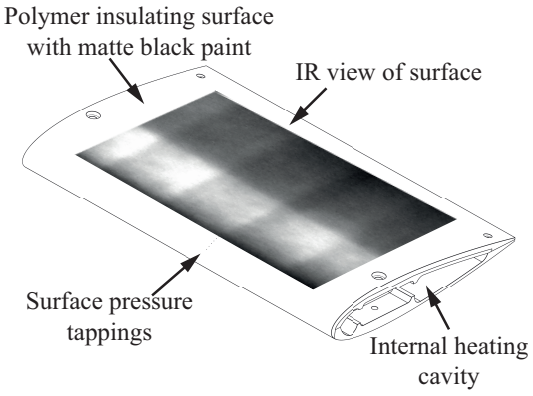


(a) Full model.

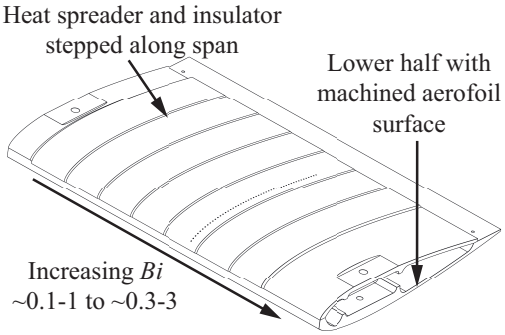


(b) Model without insulator.

**Figure 7:** CAD view of the NACA 0018 test model.

**Effect of insulator thickness**

Figure 8 shows an example of how IR thermograms are analysed. The images are split into 8 sections for the 8 steps. Traces are taken down the centre of each section and used to determine the start and end of transition from maximum and minimum temperature points, which then gives $\Delta T_{\text{lam-turb}}$.

Figure 9 shows values of $\Delta T_{\text{lam-turb}}$ from testing in two Reynolds number ranges, with analytic curves fit to the data. The agreement between the theory and experiment is excellent and is reflected across all operating conditions tested. There is an optimum Biot number that maximises SNR. The optimum Biot number is lower, with a higher optimal SNR, as Reynolds number increases. The optimum is flat in the direction of increasing Biot number, allowing for thick, low conductivity insulators to be used, and SNR drops off sharply when the insulator is too thin or conductive. At very low Biot numbers it is not possible to detect transition, with SNRs of order 1, making consideration of the thermal properties necessary.

**Effect of surface heating**

IR avoids intrusive physical instrumentation, needing only a painted surface, but heat flux through the wall may affect the flow. This section considers the effect of heating on the measurement and its intrusion on the flow features being studied.

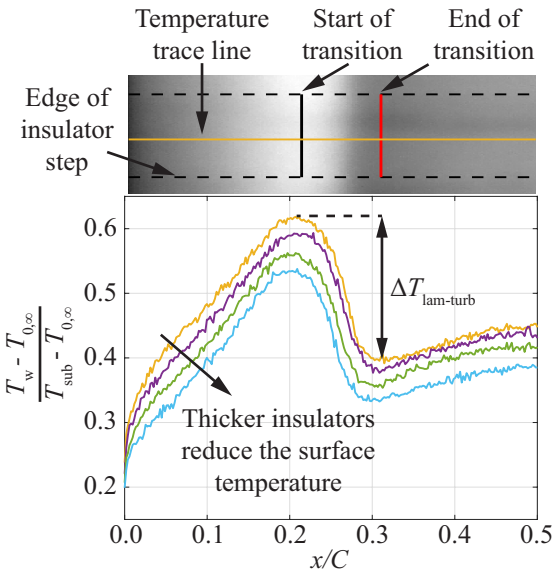


**Figure 8:** IR thermogram and temperature traces of the NACA 0018 surface showing temperature drops over transition. Only the central 4 temperature traces are shown for clarity.

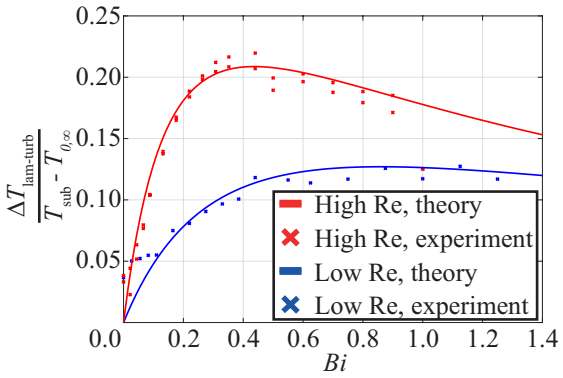


**Figure 9:** Comparison of experimental and analytic variation in $\Delta T_{\text{lam-turb}}$ for low-speed flows. Low *Re* refers to data from $Re=0.5\times10^5$, high *Re* to data from $Re=2\text{-}3\times10^5$.

Increasing heating increases SNR. Equation 6 shows that $\Delta T_{\text{lam-turb}}$ scales linearly with the substrate-fluid temperature difference. The benefits of this are shown in Fig. 10. Transition can be seen clearly with a +10K heating temperature and +20K further reduces noise around transition.

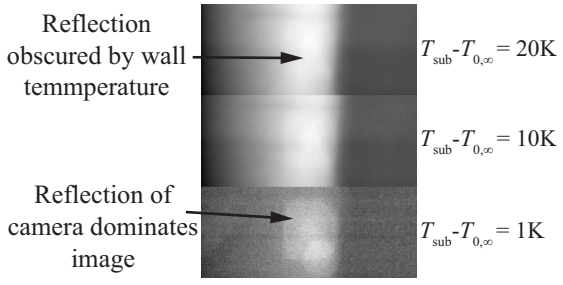


**Figure 10:** Effect of heating on IR visualisation.

An extreme case of +1K heating in Fig. 10 shows the issues faced with reduced heating. Noise is the dominant feature of the image and the

transition region is obscured by the camera reflection on the window. The reflection can be made out in the +10K image, but it does not affect the measurement. Heating temperatures below +5K produce SNRs of order 1, making reliable transition detection impossible.

Surface pressure coefficient profiles from the aerofoil are used to assess the impact of heating on the flow. If the heating is intrusive the profiles would show significant changes around separation bubbles, where heating may cause early transition. Figure 11 shows that this is not a problem. Comparing pressure profiles taken cold and with +25K of heating, the maximum safe level, there is no change in the location of separation, transition or reattachment points for both low and high Reynolds number cases. The same result is seen in IR data. This demonstrates that the level of heating required for IR visualisation is non-intrusive.

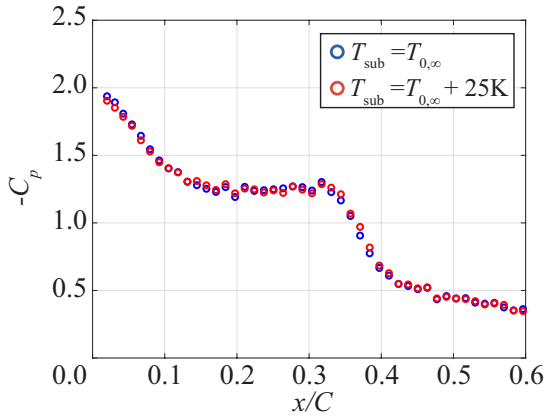


(a) $Re=1\times10^5$, $\alpha=8°$.

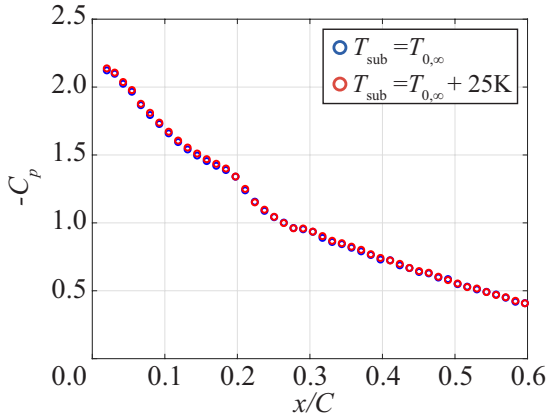


(b) $Re=4.5\times10^5$, $\alpha=8°$.

**Figure 11:** Suction surface pressure profiles comparing heated and unheated flows.

**Laminar separation bubble identification**

No distinction has yet been made between transition modes on the aerofoil. For a general measurement it does not matter, as transition in a laminar separation bubble (LSB) looks very similar to attached bypass transition in IR, with a change from low to high heat transfer coefficient. This section investigates if a distinction can be made between the two from IR alone.

Surface pressure profiles are used to identify LSBs for comparison to IR. An LSB produces a flattening of the pressure profile at the separation point with a drop at transition and reattachment [10]. Figure 12(a) shows the pressure profile over a low Reynolds number LSB compared to a, smoothed temperature profile from IR. A thermogram is shown for comparison. Transition and reattachment in the pressure and temperature profiles align well, but it is not obvious how the separation point can be determined. Qualitatively it is possible to point to the high temperature band in the thermogram and, with some intuition on the flow, suggest that it is an LSB. This has the same problems as interpreting oil flow patterns and does not give a precise separation point, with the interpretation of the thermogram depending on contrast in the colour map used.

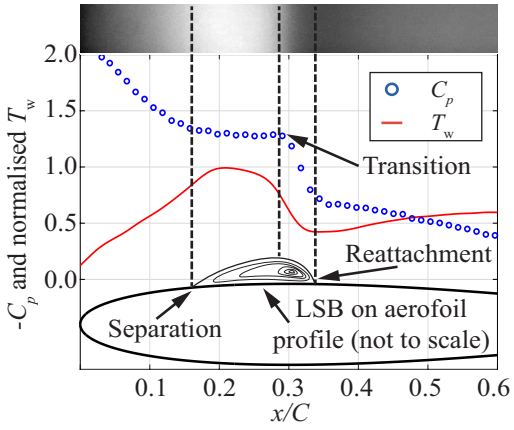


(a) Normalised surface temperature and pressure profiles over an LSB.

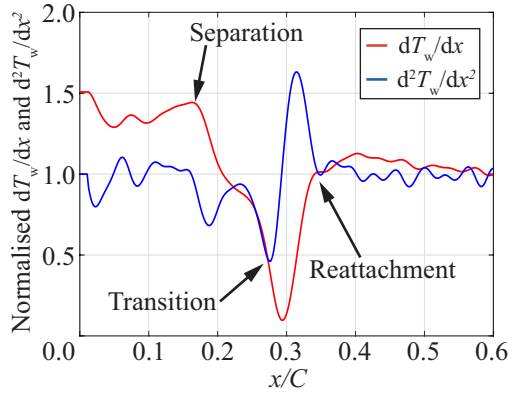


(b) First and second temperature derivatives.

**Figure 12:** Temperature, temperature derivatives and pressure over a laminar separation bubble at $Re=1.5\times10^5$, $\alpha=8°$.

A more rigorous method considers derivatives of the temperature profile. Wynnychuk and Yarusevych [11] use a peak in the first derivative to indicate separation, while Ricci and Montelpare [12] use an inflection point where the second derivative passes through zero. Figure 12(b) shows the first and second derivatives of the smoothed temperature profile. Smoothing is done with a low pass filter that preserves the overall profile and is necessary to

produce usable derivatives. There is a peak in the first derivative that aligns with the separation point in the pressure profile, however it is not a prominent one. The second derivative passes through zero at the same point, but it does so at several other points, making the inflection point criterion meaningless in this case.

The issue with using derivatives is their sensitivity to noise and non-uniformities. Even around a bubble spanning 20% of the chord there are large fluctuations in both first and second derivatives. At higher Reynolds numbers the LSB is smaller and changes are less prominent, so it isn't possible to extract features from the derivatives. Authors who have used derivatives went to additional lengths to remove non-uniformities. Wynnychuk and Yarusevych [11] used heat lamps on a polymer shell, taking 2500 images and applying a non-uniformity correction to get reliable first derivatives. Ricci and Montelpare [12] used a high performance IR camera and applied a thin-film heater to the aerofoil, coupling temperature measurements to calculations of the flow velocity to extract a Stanton number. Both studies demonstrate the feasibility of using derivatives, but the additional effort required does not facilitate rapid testing.

**Rapid testing case study**

This section presents a case study on using IR for diagnosing an unknown boundary layer state in testing. The case study looks at an aerofoil being used to investigate propulsor-wing interaction. When on an aircraft the wing operates at a Reynolds number of $3\times10^6$, however testing is at $0.2\times10^6$ due to size and speed constraints. Due to this an LSB forms on the surface of the clean wing without propulsors. The LSB is closed by the propulsor flow when they're attached. The LSB does not form at the true flight Reynolds number, so the relative change in lift and drag from the propulsors is skewed in the low Reynolds number test. A boundary layer trip is needed to close the LSB while minimising the drag rise induced by the trip. A method of visualising boundary layer state helps in identifying such a trip.

Two rapid solutions are available: oil flow visualisation or IR thermography. Both are compared in Fig. 13. The LSB is captured by both methods, with the IR showing a high temperature band where the oil pools up. The IR gives a clear visualisation over the whole wing, whereas the oil is streaky due to it running before and after the test. The oil also changes the topology of the LSB. The non-zero thickness of the film trips the boundary layer early and shortens the bubble compared to the non-intrusive IR.

The wing was not designed for IR, however as it is polymer and has a black surface it is well suited to the method. Installing a heater is not necessary for diagnosis, so a transient temperature change is used. The wing's surface was initially heated with a hot air gun but use of an air cooler gives a higher temperature difference as the polymer can withstand low temperatures. A FLIR A615 IR camera is used, with the whole IR set up taking less than 30 minutes from the start to the thermogram in Fig. 13. A full sweep of incidence is possible without needing to be reheated or cooled. The oil-dye mixture takes multiple iterations to produce a usable result, with each iteration and incidence requiring unpleasant cleaning, re-mixing and reapplying of the oil over several hours or days.

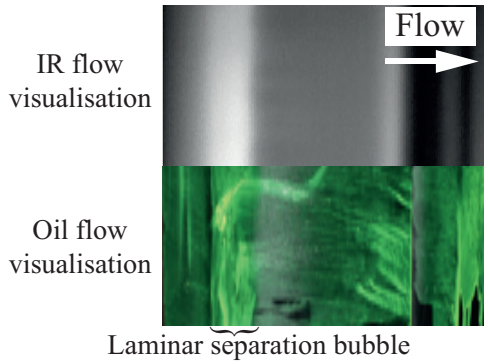


**Figure 13:** Comparison of oil flow and IR visualisation of a separation bubble over a low Reynolds number aerofoil [13].

Distributed roughness elements in the form of silica beads attached with a water soluble adhesive are used to find the minimal trip to close the LSB. Strips of different bead sizes are placed along the span to find the critical size. Figure 14 shows an IR visualisation of beads on the NACA 0018 aerofoil from previous tests. The 200 µm beads hardly affect the boundary layer, causing a slight advance in transition downstream. The 250 µm beads have a stronger effect, partially tripping the boundary layer before full transition shortly after. The 300 µm beads cause immediate transition and are able to close the LSB on the distributed propulsor aerofoil.

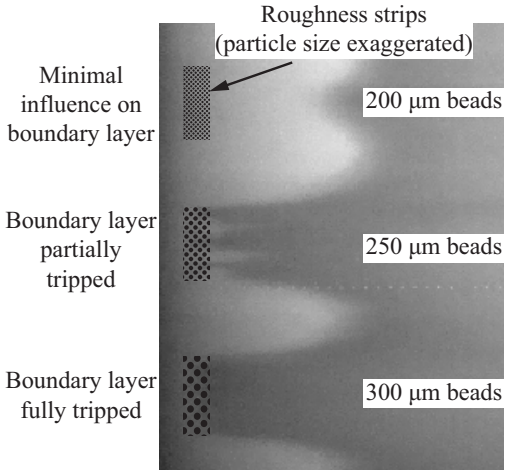


**Figure 14:** Effect of different roughness element sizes for boundary layer tripping.

This case study shows the value of IR in a rapid testing environment. It enables fast movement from uncertainty in the boundary layer state and its effect on the experiment through to a complete solution without additional instrumentation or modification to the experiment.

## HIGH-SPEED EXPERIMENTS

This section describes ongoing work to validate high-speed modelling of transition measurements that utilise recovery temperature differences. This takes a similar form to low-speed validation, with the insulator thickness varied in a range of conditions to assess its effect on the measurement.

An additional aspect to the high-speed testing is its aim of validating the method for use in a high TRL rotating transonic compressor test, which features a shock-boundary layer interaction. This can be visualised in IR due to the drop in Mach number and the boundary layer change through the shock, which causes separation and transition in a laminar boundary layer and a thickening of a turbulent one. As the compressor is rotating there are limits on the substrate material and camera integration time due to structural and motion blur requirements. This constrains the insulator thickness and increases the NETD of the IR camera, limiting the maximum SNR achievable. The rotation of the compressor also increases the relative stagnation temperature of the flow, effectively heating the model and amplifying the effect of the change in heat transfer coefficient. This work investigates the impact the insulator and substrate material have on visualisation to find the minimum requirements for a successful measurement.

### Experimental design

Experimental design must produce a range of boundary layer behaviours at high subsonic and transonic Mach numbers. The overall layout of the test rig is shown in Fig. 15(a). The tunnel has an atmospheric inlet and is connected to the Nash vacuum pump at the Whittle Laboratory, which has a mass flow capacity of 0.43 kg s$^{-1}$. An 8.5:1 contraction leads to a turbulence grid and a 45 mm × 45 mm working section. A detailed view of the working section is shown in Fig. 15(b).

The test model has an aerofoil profile on one side and is mounted to a plate, which forms one wall of the working section. The model can be manufactured from any material including polycarbonate, aluminium, titanium and stainless steel. Varying thicknesses of black paint are applied as the insulator. Bleed slots upstream of the working section and at the model's leading edge allow Mach number and incidence to be varied using valves in the bleed path. The bleed leads to a downstream throat to provide a pressure margin.

Surface tappings on one wall and a pitot probe provide isentropic Mach number measurements. A set of pressure tappings are clustered closer to the model surface to capture shocks. An optical window is placed in the opposite wall for background oriented schlieren visualisation of the flow. Thermocouples in the flow and embedded in the end walls give thermal boundary conditions for use in finite element analysis. An IR window gives a view of the model for a FLIR SC7300LW, a high-performance IR camera with a resolution of 320 × 256 pixels, a spectral range of 7.7-9.3 µm and an NETD of 14 mK. The camera integration time can be reduced to 3 µs, allowing it to take snapshots of a rotating blade with minimal motion blur. The low integration time results in more noise, so integration time is a trade-off between noise and blur.

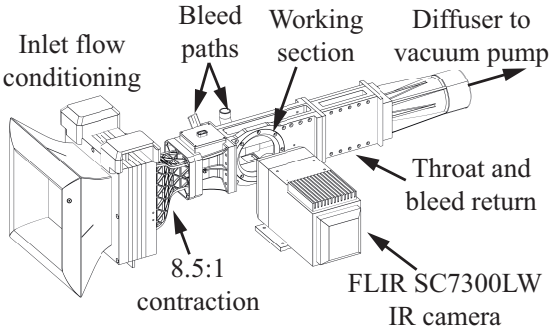


(a) Full rig.

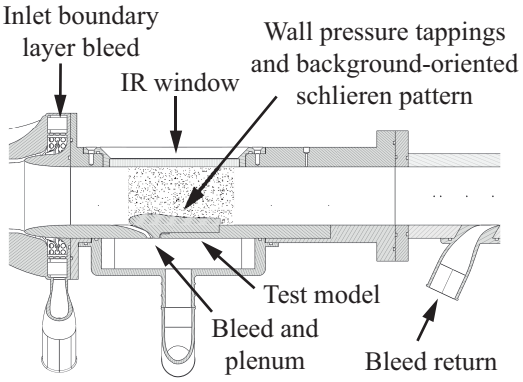


(b) Working section.

**Figure 15:** CAD view of the high-speed test section.

### Preliminary results

A thermogram taken during commissioning of the experiment is shown in Fig. 16. Features labelled are yet to be verified but are representative of the view of a shock-boundary layer interaction. This image is from runs using a 3D printed model and long integration times, and so is not representative of the challenges associated with a rotating compressor visualisation.

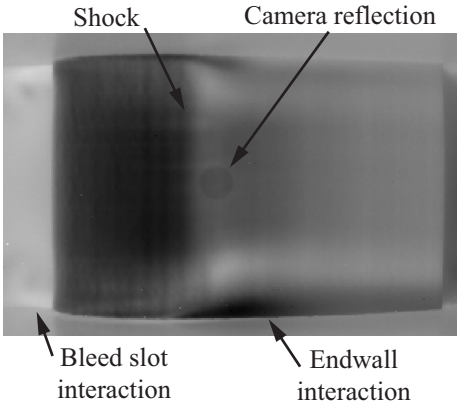


**Figure 16:** IR thermogram of a shock-boundary layer interaction on the test piece surface.

## CONCLUSIONS

This paper demonstrates the value of IR thermography for boundary layer visualisation in rapid testing. A 1D analytic model of the temperature change over transition shows the scope for optimisation in measurements and the possible pitfalls in experimental design. Low-speed experiments validate the theory, showing that SNR can be optimised with the correct thermal design without intrusion into the flow. Identification of separation bubbles in IR is shown to be possible but requires some interpretation of thermographic results. A case study on the use of IR in rapid testing is presented, demonstrating how IR can be used at speed to diagnose unknown boundary layer states and fix experimental issues associated with low Reynolds number testing. Current work on validation of high-speed 1D analysis is previewed, with an emphasis on the use of IR for visualisation in an industrial rotating transonic compressor test.

### Future work

Experimental work discussed in this paper validates the 1D analysis but is limited in the data it can extract to help inform IR method development. Future work will therefore include computational studies on the flow and conduction in the model. High fidelity CFD of separation bubbles in low and high-speed flows will be used to develop understanding of the expected heat transfer and recovery temperature profiles seen in IR. Finite element analysis will be used to investigate transient effects and the impact of lateral conduction within the model on visualisation. Additional experimental work will also be performed in a variable density facility, allowing Mach and Reynolds numbers to be varied independently and approach the true conditions in a transonic compressor.

## ACKNOWLEDGMENTS

The authors would like to thank Mitsubishi Heavy Industries for their generous financial support, with particular thanks to Yoshiyuki Okabe. Thanks also go to Bram Hulhoven for the use of his high-speed wind tunnel, George Hawkswell for allowing us to test IR methods on his distributed aerofoil, Dr Chris Clark for his helpful discussion throughout and finally to Liam Cohen and Oliver Wadsworth for their manufacturing work.

## NOMENCLATURE

### Roman symbols

| | |
|---|---|
| $Bi$ | Biot number |
| $C$ | Chord, m |
| $C_p$ | Pressure coefficient |
| $d$ | Insulator thickness, m |
| $h$ | Heat transfer coefficient, $Wm^{-2}\ K^{-1}$ |
| $M$ | Mach number |
| $Nu$ | Nusselt number |
| $Pr$ | Prandtl number |
| $\dot{q}$ | Heat flux, $Wm^{-2}$ |
| $Re$ | Reynolds number |
| $r$ | Recovery factor |
| $T$ | Temperature, K |
| $y$ | Wall normal distance, m |
| $x$ | Chord-wise distance, m |

### Greek symbols

| | |
|---|---|
| $\alpha$ | Incidence, ° |
| $\gamma$ | Ratio of specific heats |
| $\lambda$ | Thermal conductivity, $Wm^{-1}\ K^{-1}$ |

### Subscripts

| | |
|---|---|
| 0 | Stagnation |
| $\infty$ | Free stream |
| lam | Laminar |
| opt | Optimum |
| rec | Recovery |
| sub | Substrate |
| turb | Turbulent |
| w | Wall |

### Abbreviations

| | |
|---|---|
| CAD | Computer Aided Design |
| IR | InfraRed |
| LSB | Laminar Separation Bubble |
| NETD | Noise-Equivalent Temperature Difference |
| SNR | Signal-to-Noise Ratio |
| TRL | Technology Readiness Level |

## REFERENCES

[1] Mayle, R. E. (1991), "The Role of Laminar-Turbulent Transition in Gas Turbine Engines," Journal of Turbomachinery, **113**(4), pp. 509–536.

[2] Kalfas, A. I. (1994), "Transition to Turbulence in the Boundary Layer of Turbomachinery Blading," PhD thesis, Cranfield University.

[3] Poels, A., Rudmin, D., Benaissa, A., Poirel, D. (2015), "Localization of Flow Separation and Transition Over a Pitching NACA0012 Airfoil at Transitional Reynolds Numbers Using Hot-Films", Journal of Fluids Engineering, **137**(2), p. 12450.

[4] Peake, D. J., Bowker, A. J., Lockyear, S. J., and Ellis, F. A. (1977), "Non-obtrusive Detection of Transition Region Using an Infra-red Camera," NATO Advisory Group for Aerospace Research and Development, AGARD-CP-224.

[5] Mori, M. and Novak, L. and Sekavčnik, M. (2007), "Measurements on Rotating Blades Using IR Thermography," Experimental Thermal and Fluid Science, **32**(2), pp. 387-396.

[6] Joseph, L. A., Borgoltz, A., and Devenport, W. (2016), "Infrared Thermography for Detection of Laminar-Turbulent Transition in Low-Speed Wind Tunnel Testing," Experiments in Fluids, **57**(5), p. 77.

[7] Shapiro, A. H. (1954), *The Dynamics and Thermodynamics of Compressible Fluid Flow*, Vol. 2, Krieger, Malabar, USA.

[8] Gerakopulos, R., Boutilier, M. S. H., and Yarusevych, S. (2010), "Aerodynamic Characterization of a NACA 0018 Airfoil at Low Reynolds Numbers," in 40th AIAA Fluid Dynamics Conference and Exhibit, Paper No. AIAA 2010-4629.

[9] Protolabs (2020). "Stereolithography ABS-Like Grey Supplier Data Sheet: Accura Xtreme," manufacturer data sheet.

[10] Popov, A. V., Botez, R. M., and Labib, M. (2008), "Transition Point Detection from the Surface Pressure Distribution for Controller Design," Journal of Aircraft, **45**(1), pp. 23-28.

[11] Wynnychuk, D. W., and Yarusevych, S. (2020), "Characterization of Laminar Separation Bubbles Using Infrared Thermography," AIAA Journal, **57**(7), pp. 2831-2843.

[12] Ricci, R. and Montelpare, S. (2009), "Analysis of Boundary Layer Separation Phenomena by Infrared Thermography," Quantitative InfraRed Thermography Journal, **6**(1), pp. 101-125.

[13] Hawkswell, G. (2022), personal communication, Whittle Laboratory, University of Cambridge.